Available online at www.sciencedirect.com
ScienceDirect
Ultrasonics 46 (2007) 205–218
Ultrasonics
www.elsevier.com/locate/ultras

Dynamic modeling and experimental verification of a piezoelectric part feeder in a structure with parallel bimorph beams

Paul C.-P. Chao [a,*], Chien-Yu Shen [b]

[a] Department of Electrical and Control Engineering, National Chiao Tung University, Hsinchu 300, Taiwan, ROC
[b] Department of Mechanical Engineering, Chung-Yuan Christian University, Chung-Li 32023, Taiwan, ROC

Received 6 September 2006; received in revised form 28 January 2007; accepted 4 February 2007
Available online 12 February 2007

Abstract

The study is aimed to perform dynamic modeling of a part feeder powered by piezoelectric actuation. This part feeder consists mainly of a horizontal platform vibrated by a pair of parallel piezoelectric bimorph beams. Owing to intermittent impacts with the platform, the transported part on the platform is able to march forward from one end to another. Dynamic modeling of the feeder is accomplished by essentially using the Rayleigh–Ritz decomposition method. The process of modeling first incorporates material properties and constitutive equations of the piezoelectric materials, and then captures the complex dynamics of the parallel-beam piezo-feeder by three low-order assumed-modes in the transverse direction of the vibrating beams. Applying Lagrange's equations on the kinetic and strain energies formulated in terms of generalized coordinates associated with the first three modes, the system dynamics is then represented by three coupled discrete equations of motion. Based on these equations, motions of the platform can be obtained. With platform motion in hand, the intermittent impacts between the parts and the platform are modeled, rendering the marching speed of the part. Numerical simulations are conducted along with the experiments. The closeness found between the theoretical predicted transporting speed of the part and the experimental counterparts verify the effectiveness of the models established.

Keywords: Piezoelectric bimorph beam; Part feeder; Rayleigh–Ritz method

1. Introduction

Piezoelectric part feeders in varied structures are often used nowadays to transport small parts such as screws, nuts and IC components along a manufacture line in many automatic factories, especially those in semi-conductor industry. These piezoelectric feeders own merits of low cost, simple structure and free of electromagnetic effects. This study is dedicated to establish a dynamic model and perform dynamic analysis on the piezoelectric feeder in a simple form as shown in Fig. 1—a rectangular platform supported by a pair of parallel bimorph piezoelectric bimorph beams tilted by some angle. Applying harmonic voltages on the two piezoelectric beams in a synchronous fashion, the platform would be in pure translational motions in the direction perpendicularly to the lengths of the piezo-beams. The parts to be transported on the platform are then moved forward to another end of the platform by intermittent contacts/collision with the platform.

The modeling of the bimorph piezoelectric beam has been intensively investigated in the recent years. Some research works focused on incorporating nonlinear factors into the lumped model of the beam dynamics [1–3], while others further developed various control schemes to achieve precision positioning or reduce structure vibrations via piezoelectric structures [4–12]. Within these works, Choi et al. [6–9] proposed control designs for piezoelectric beams to perform position tracking. The designs were based on the discrete beam model derived from assumed-modes. Gosavi and Kelkar [10] constructed the model of

* Corresponding author. Tel.: +886 3 5131377; fax: +886 3 5752469.
E-mail address: pchao@mail.nctu.edu.tw (P.C.-P. Chao).

0041-624X/$ - see front matter © 2007 Elsevier B.V. All rights reserved.
doi:10.1016/j.ultras.2007.02.002

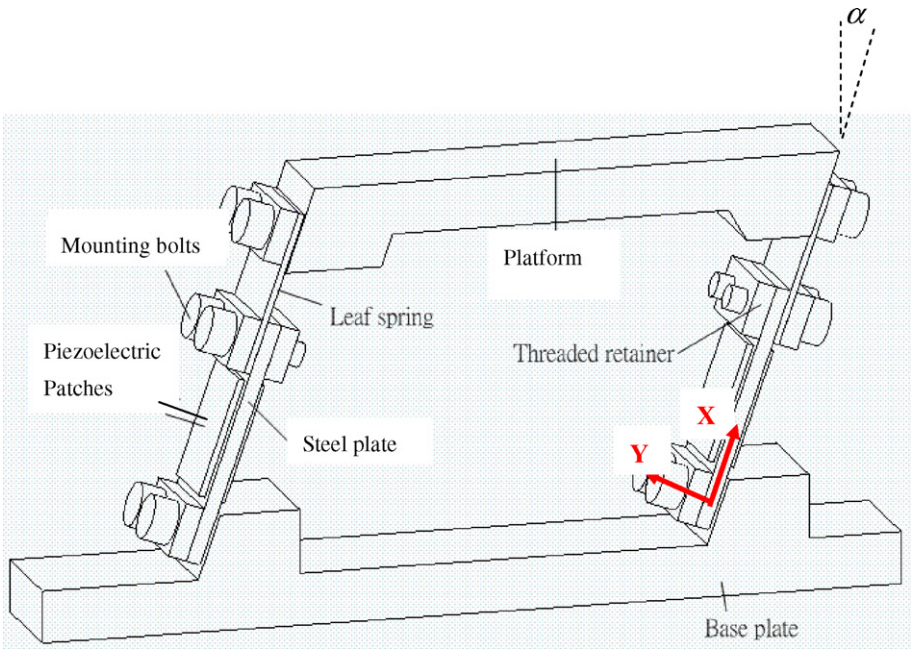

Fig. 1. The physical structure of the piezoelectric feeder.

a piezo-actuated flexible beam by Lagrangian formulation for robust control design. Han et al. [11] developed an analytical model of the laminated composite beam by classical laminated beam theory and Ritz method. Bailey et al. [12] designed an active vibration damper for a cantilever beam by a piezoelectric polymer and distributed-parameter control theory. Recently, efforts were paid to utilize the technique of finite elements to model the piezo-structures. Piefort and Preumont [13] modeled coupled piezoelectrical systems by finite element formulation. Cappelleri et al. [14] constructed finite element simulations of the PZT bimorph actuators with aim for computational inexpensiveness. Fung et al. [15] and Fung and Chao [16] modeled the dynamic behavior of the piezoelectric beams by Hamilton's principle and the finite elements.

Besides the past studies on the dynamics of piezo-beams in varied forms, few research works devote effort on piezoelectric part feeder. Choi and Lee [17] conducted modal analysis and control of a bowl parts piezo-feeder. Jiang et al. [18] developed a simulation software for parts feeding. Doi et al. [19] achieved feedback control of a parallel beam parts feeder; however, the main focus was on the controller development and thus the associated modeling derived only lumped model and the collision between parts and feeder were not explored. In this study, the method of Rayleigh–Ritz decomposition featuring assumed modes [20] is employed herein to predict dynamics of parallel piezoelectric beams, then using basic collision theory [21] to estimate transporting speed of the part on the platform. The transporting velocity of the objective on the feeder platform depends on various designs of the feeder such as sizes/mass/material properties of piezoelectric beams and platform, even that the tilting angle of the two parallel piezo-beams has profound effects on the transporting velocity. The final goal of the current study is to establish reliable theoretical models for designers to predict well about the feeder performance—the transporting velocity, prior to mass production. Experiments are conducted to verify the theoretically-predicted transportation speeds of the part. General closeness between simulation data and experiment counterparts are found, which verify the effectiveness of the models developed.

2. Dynamic modeling

The physical structure of the piezo-feeder as well as denotations of components is shown in Fig. 1. The main components include (1) a horizontal platform carrying transported parts, (2) two parallel bimorph piezoelectric beams, each of which has leaf spring bolted with a steel plate sandwiched by piezoelectric patches. With the beams tilted by an angle α from vertical, the parallel beams would be flexurally deformed reciprocally with harmonic voltages applied on piezoelectric patches. The platform is consequently in pure translational motions perpendicular to the lengths of the piezo-beams. The assumption of synchronism in planar movements of two beams regardless of manufacturing tolerance is set to initialize the ensuing dynamic modeling. This assumption keeps the platform in constant horizontal while vibrating. The dynamics of the beams are analyzed first in the following subsection to predict platform motion, which is followed by experimental model verification in Section 2.2. Subsequently, the impact dynamics of the part to the platform is analyzed to predict transporting speed in Section 2.3.

2.1. Bimorph piezoelectric beams

A simplified model of a piezoelectric bimorph beam is shown in Fig. 2, one end of which is fixed to baseplate (ground) while another is in oscillatory vibrations with a constant angle α to the horizontal. Fig. 2a denotes important dimensions and coordinates, where L is the total length of the piezo-beam; L_1 is the length of portion of the steel plate sandwiched by piezo-patch; x is the axis along the beam while y captures the transverse deflection of the beam at given instant; i.e., $y = y(x, t)$. Fig. 2b shows all forces acting on the beam. In both Fig. 2a,b, the platform and mounting bolts are simplified as point masses and located at appropriate positions. The two piezoelectric patches on the steel plate produce a harmonic bending moment M_v. The moment results in harmonic motion of the entire beam, rendering the horizontal platform vibrating in pure harmonic translational motions with a constant angle α to the horizontal and then moving the part on the platform forward by the impacts between the part and platform. The objective of the analysis in this section is to fetch the harmonic motion of the platform by performing dynamic modeling of the piezoelectric bimorph beam to obtain the motion of the beam tip before analyzing the impact dynamic of the transported part to the platform in the following section.

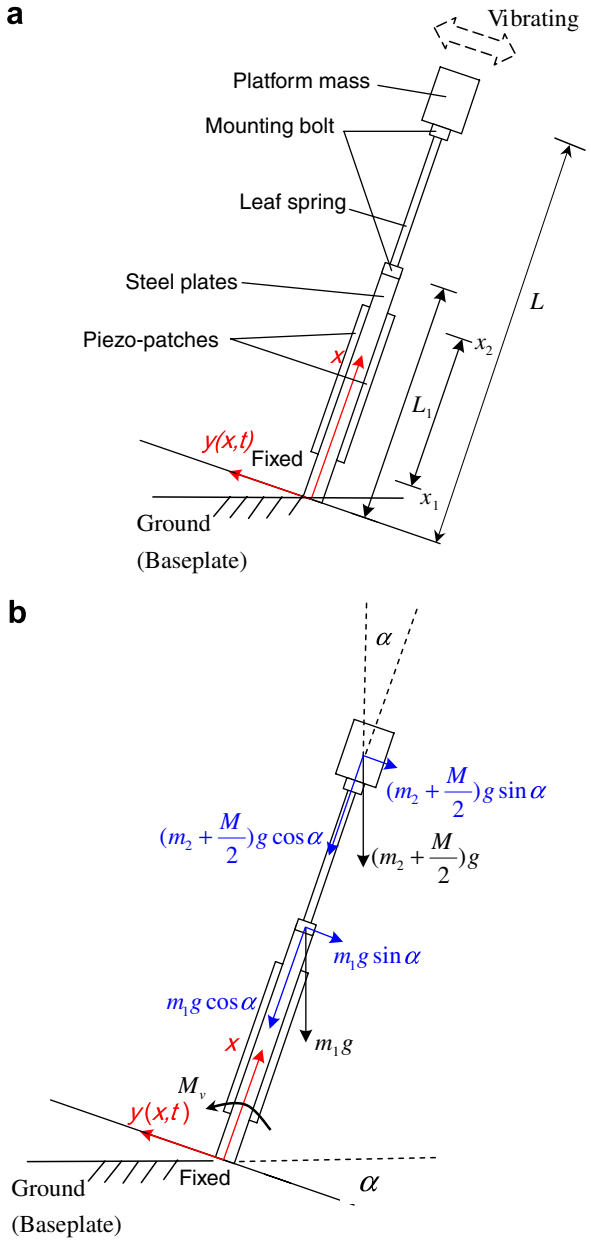

Fig. 2. (a) The configuration and each component of the simplified model and (b) acting forces on the piezo-beam.

The dynamic modeling of the piezoelectric bimorph beams is carried out via the method of the assumed-mode accompanied with the technique of Rayleigh–Ritz decomposition [20] and linear constitutive physical laws of the piezoelectric materials. It is first assumed the piezo-beams are primarily in flexural motion, with negligible axial motion. Based on the method of the assumed-mode, the flexural motions of the beam $y(x, t)$ as defined in Fig. 2 can be approximated by

$$y(x,t) = \sum_{i=1}^{n} \phi_i(x) q_i(t), \tag{1}$$

where $\phi_i(x)$ is the assumed-mode shape function, $q_i(t)$ is the generalized temporal modal coordinate, and n is the number of modes. The associated boundary conditions of the beam are

$$y(x,t) = 0, \quad x = 0 \quad \text{and} \quad y'(x,t) = 0, \quad x = 0, \tag{2a}$$

to reflect the fixed end at the bottom, while

$$y'(x,t) = 0, \quad x = L \quad \text{and} \quad y'''(x,t) = 0, \quad x = L \tag{2b}$$

to realize the condition of the fixed tilt angle α and free shear force at the other end, respectively. This non-zero fixed angle of α in fact makes possible horizontal, pure translational motions of the platform. It should be noted at this point that since the piezoelectric beam of feeder is not only fixed to ground but also connected to the horizontal platform with a fixed tilt angle, the ensuing modeling process is unique and different from those for piezoelectric cantilever beams, which were well done in many past works [6–10]. Satisfying the four boundary conditions in Eq. (2), the trail functions for applying the assumed-mode method are set as the mode shapes, which are

$$\phi_i(x) = (\sin\beta_i x - \sinh\beta_i x) + \alpha_i(\cos\beta_i x - \cosh\beta_i x), \quad i = 1, 2, \ldots, \tag{3}$$

where

$$\alpha_i = \frac{(\cos\beta_i L - \cosh\beta_i L)}{(\sin\beta_i L + \sinh\beta_i L)}$$

and the values of β_i's can be easily calculated by $\tan\beta_i L + \tanh\beta_i L = 0$. Note that one can follow a standard procedure of solving vibration of a beam [20] to obtain the mode

shapes in Eq. (3). With calculated β_i's the first three mode shapes of $\phi_i(x)$ are depicted in Fig. 3, which would be utilized later in this study. The kinetic energy of the system can then be expressed as

$$T(t) = \frac{1}{2}\int_0^{L_1} m_b(x)\dot{y}^2(x,t)\,dx + \frac{1}{2}\int_{x_1}^{x_2} m_p(x)\dot{y}^2(x,t)\,dx + \frac{1}{2}m_1\dot{y}^2(L_1,t) + \frac{1}{2}\int_{L_1}^{L} m_s(x)\dot{y}^2(x,t)\,dx + \frac{1}{2}\left(m_2 + \frac{M}{2}\right)\dot{y}^2(L,t), \quad (4)$$

where $m_b(x)$, $m_p(x)$ and $m_s(x)$, respectively, denote the masses of steel beam, piezoceramic and leaf spring, while m_1 and m_2 are the mass of mounting bolts and M is the mass of the horizontal platform. It can be seen from the term of $M/2$ in Eq. (4) that the total mass of the platform is evenly distributed at two beam tips. Incorporating Eq. (1) into Eq. (4) yields

$$T(t) = \frac{1}{2}\sum_{i=1}^{n}\sum_{j=1}^{n} m_{ij}\dot{q}_i(t)\dot{q}_j(t), \quad (5)$$

where

$$m_{ij} = m_{ji} = \int_0^{L_1} m_b(x)\phi_i(x)\phi_j(x)\,dx + \int_{x_1}^{x_2} m_p(x)\phi_i(x)\phi_j(x)\,dx + m_1\phi_i(L_1)\phi_j(L_1) + \int_{L_1}^{L} m_s(x)\phi_i(x)\phi_j(x)\,dx + \left(m_2 + \frac{M}{2}\right)\phi_i(L)\phi_j(L), \quad i,j = 1,\ldots,n. \quad (6)$$

Assuming small deflections of the piezo-beams and the constant cross section along the length, the bending moment induced is

$$Mom(x,t) = \frac{E_b I_b(x)\partial^2 y(x,t)}{\partial x^2}, \quad (7)$$

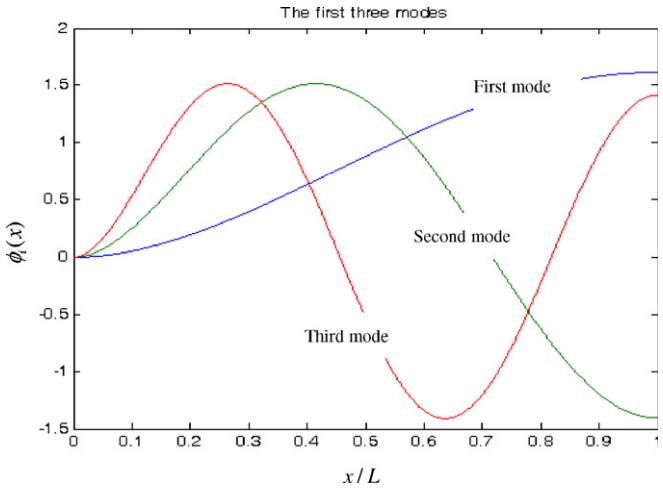

Fig. 3. The first three assumed-modes of the piezo-beam.

where E_b and I_b are Young's modulus and moment of inertia of the steel beam, respectively. The strain energy of steel beam is

$$V_b(t) = \frac{1}{2}\int_V \sigma_b\varepsilon_b\,dV, \quad (8)$$

where σ_b and ε_b are stress and strain of the beam, respectively, and they are functions of axial position x only. The stress can be expressed in terms of the bending moment as

$$\sigma_b(x,t) = -\frac{Mom\cdot y(x,t)}{I(x)}. \quad (9)$$

Incorporating Eqs. (7) and (9) into Eq. (8), and using Hooke's law ($\sigma_b = E_b\varepsilon_b$) yield

$$V_b(t) = \frac{1}{2}\int_0^{L_1} E_b I_b(x)\left(\frac{\partial^2 y(x,t)}{\partial x^2}\right)^2 dx, \quad (10)$$

where $I_b = \frac{b_b h_b^3}{12}$ with b_b and h_b being width and thickness the steel beam, respectively. Consider the linear constitutive equations for piezoelectric materials in the form of

$$\sigma_{11} = c^D\delta_{11} - h_{31}D, \quad (11)$$

$$E_3 = -h_{31}\delta_{11} + \beta_{33}D, \quad (12)$$

where σ_{11} and δ_{11} are the stress and strain in the axial direction of piezoelectric elements; E_3 is the applied electric field and D is the electric displacement which is positive when the electric field and the polarization are in the same direction. c^D, h_{31} and β_{33} are the elastic stiffness for constant electric displacement, the piezoelectric strain constant and dielectric constant, respectively. The strain energy of the two piezoelectric patches in the bimorph structure is then

$$V_p(t) = \frac{1}{2}\int_{V_L}(\sigma_{11}\delta_{11} + DE_3)\,dV + \frac{1}{2}\int_{V_R}(\sigma_{11}\delta_{11} + DE_3)\,dV, \quad (13)$$

where V_L and V_R are individual volumes of the two piezo-patches at right and left sides of the steel plate, respectively. Substituting Eqs. (11) and (12) into Eq. (13) and also incorporating Eqs. (7) and (9), $V_p(t)$ arrive at

$$V_p(t) = \int_{x_1}^{x_2}\frac{E_p^2 I_p}{c^D}\left(\frac{\partial^2 y(x,t)}{\partial x^2}\right)^2 dx - A_p\int_{x_1}^{x_2}\frac{h_{31}^2 D^2}{c^D}dx + A_p\int_{x_1}^{x_2}\beta_{33}D^2\,dx, \quad (14)$$

where $I_p = \frac{b_p h_p^3}{12} + A_p d_{bp}^2$ with E_p, b_p, h_p and I_p being the Young's modulus, width, thickness and the moment of inertia of the piezo-patch, respectively, and finally d_{bp} is the distance between the neutral axes of the steel and the piezo-patches. On the other hand, the strain energy of the leaf spring is

$$V_s(t) = \frac{1}{2}\int_{L_1}^{L} E_s I_s(x)\left(\frac{\partial^2 y(x,t)}{\partial x^2}\right)^2 dx. \quad (15)$$

The total strain energy of the entire beam system including the masses of platform and mounting bolts can be obtained as

$$V(t)=\frac{1}{2}\int_0^{L_1}E_bI_b(x)\left(\frac{\partial^2y(x,t)}{\partial x^2}\right)^2dx+\int_{x_1}^{x_2}\frac{E_p^2I_p}{c^D}\left(\frac{\partial^2y(x,t)}{\partial x^2}\right)^2dx-A_p\int_{x_1}^{x_2}\frac{h_{31}^2D^2}{c^D}dx+A_p\int_{x_1}^{x_2}\beta_{33}D^2dx+\frac{1}{2}\int_{L_1}^{L}E_sI_s(x)\left(\frac{\partial^2y(x,t)}{\partial x^2}\right)^2dx+m_1g\cos\alpha\cdot L_1\left(\frac{(y'(L_1,t))^2}{2}\right)+\left(m_2+\frac{M}{2}\right)g\cos\alpha\cdot L\left(\frac{(y'(L,t))^2}{2}\right). \tag{16}$$

Substituting Eq. (1) into Eq. (16), the total strain energy $V(t)$ can further be expressed as

$$V(t)=\frac{1}{2}\sum_{i=1}^{n}\sum_{j=1}^{n}k_{ij}q_i(t)q_j(t)-A_p\int_{x_1}^{x_2}\frac{h_{31}^2D^2}{c^D}dx+A_p\int_{x_1}^{x_2}\beta_{33}D^2dx+\sum_{i=1}^{n}\sum_{j=1}^{n}m_1g\cos\alpha\cdot L_1\left(\frac{\phi_i'(L_1)\phi_j'(L_1)}{2}\right)q_i(t)q_j(t)+\sum_{i=1}^{n}\sum_{j=1}^{n}\left(m_2+\frac{M}{2}\right)g\cos\alpha\cdot L\left(\frac{\phi_i'(L)\phi_j'(L)}{2}\right)q_i(t)q_j(t), \tag{17}$$

where

$$k_{ij}=k_{ji}=\int_{L_1}E_bI_b\left[\left(\frac{\partial^2\phi_i(x)}{\partial x^2}\right)\left(\frac{\partial^2\phi_j(x)}{\partial x^2}\right)\right]dx+2\int_{x_2-x_1}\frac{E_p^2I_p}{c^D}\left[\left(\frac{\partial^2\phi_i(x)}{\partial x^2}\right)\left(\frac{\partial^2\phi_j(x)}{\partial x^2}\right)\right]dx+\int_{L-L_1}E_sI_s\left[\left(\frac{\partial^2\phi_i(x)}{\partial x^2}\right)\left(\frac{\partial^2\phi_j(x)}{\partial x^2}\right)\right]dx,\quad i,j=1,\ldots,n. \tag{18}$$

With mass and stiffness matrices derived as in Eqs. (6) and (18), respectively. The external work done by the applied voltage and gravity is derived next, which is started with expressing the work as

$$W=M_v(t)\cdot[y'(x_2,t)-y'(x_1,t)]+m_1g\sin\alpha\cdot y(L_1,t)+\left(m_2+\frac{M}{2}\right)g\sin\alpha\cdot y(L_2,t), \tag{19}$$

where $M_v(t)$ is the bending moment generated by the piezoceramic bimorph patches due to the application of harmonic voltage $\tilde{V}(t)$. In fact,

$$M_v(t)=-2\varepsilon_pE_ph_pb_p\left(\frac{h_p+h_b}{2}\right)=c\cdot\tilde{V}(t), \tag{20}$$

where ε_p is the induced strain in the piezoceramic patches, which is arisen from application of the input voltage. The proportionality of ε_p to applied voltage $\tilde{V}(t)$ in fact makes possible the expression of $M_v(t)=c\cdot\tilde{V}(t)$ in the second line of Eq. (20), where c is a constant and can be seen as the generated bending moment per voltage. The work in Eq. (19) can further be expressed in terms of generalized coordinates of the assumed modes in Eq. (1) as

$$W=\sum_{i=1}^{n}M_v(t)\cdot[\phi_i'(x_2)-\phi_i'(x_1)]q_i(t)+\sum_{i=1}^{3}m_1g\sin\alpha\cdot\phi_i(L_1)q_i(t)+\sum_{i=1}^{n}\left(m_2+\frac{M}{2}\right)g\sin\alpha\cdot\phi_i(L)q_i(t). \tag{21}$$

With the kinetic/potential energies and work obtained, the Lagrangian can be formulated by summing Eqs. (4), (17) and (21), which is prepared for further derivation of system equations of motion, yielding

$$\hat{L}=T-V+W=\frac{1}{2}\sum_{i=1}^{n}\sum_{j=1}^{n}m_{ij}\dot{q}_i(t)\dot{q}_j(t)-\frac{1}{2}\sum_{i=1}^{n}\sum_{j=1}^{n}k_{ij}q_i(t)q_j(t)+A_p\int_{x_1}^{x_2}\frac{h_{31}^2D^2}{c^D}dx-A_p\int_{x_1}^{x_2}\beta_{33}D^2dx-\sum_{i=1}^{n}\sum_{j=1}^{n}m_1g\cos\alpha\cdot L_1\left(\frac{\phi_i'(L_1)\phi_j'(L_1)}{2}\right)q_i(t)q_j(t)-\sum_{i=1}^{n}\sum_{j=1}^{n}(m_2+\frac{M}{2})g\cos\alpha\cdot L\left(\frac{\phi_i'(L)\phi_j'(L)}{2}\right)q_i(t)q_j(t)+\sum_{i=1}^{n}M_v(t)\cdot[\phi_i'(x_2)-\phi_i'(x_1)]q_i(t)+\sum_{i=1}^{n}m_1g\sin\alpha\cdot\phi_i(L_1)q_i(t)+\sum_{i=1}^{n}\left(m_2+\frac{M}{2}\right)g\sin\alpha\cdot\phi_i(L)q_i(t). \tag{22}$$

Using Lagrange's equations

$$\frac{d}{dt}\left(\frac{\partial\hat{L}}{\partial\dot{q}_i(t)}\right)-\frac{\partial\hat{L}}{\partial q_i(t)}=0,\quad i=1,\ldots,n, \tag{23}$$

one can derive the discrete equations of motion for the system as

$$\sum_{j=1}^{n}m_{ij}\ddot{q}_j(t)+\sum_{j=1}^{n}k_{ij}q_j(t)+\sum_{j=1}^{n}m_1g\cos\alpha\cdot L_1\phi_i'(L_1)\phi_j'(L_1)q_j(t)+\sum_{j=1}^{3}\left(m_2+\frac{M}{2}\right)g\cos\alpha\cdot L\phi_i'(L)\phi_j'(L)q_j(t)=M_v(t)\cdot[\phi_i'(x_2)-\phi_i'(x_1)]+m_1g\sin\alpha\cdot\phi_i(L_1)+\left(m_2+\frac{M}{2}\right)g\sin\alpha\cdot\phi_i(L). \tag{24}$$

Note that an additional Lagrange's equation governing the electric displacement D other than those in Eq. (23) is not considered herein since it leads to no mechanical dynamic equation due to the fact that the piezoelectric effects are already incorporated in mechanical work in Eq. (21) through the moment $M_v(t)$. To re-arrange Eq. (24) into standard forms of dynamic equations, define

$$M_{ij}=m_{ij},\quad \text{and} \tag{25}$$

$$K_{ij}=k_{ij}+m_1g\cos\alpha\cdot L_1\phi_i'(L_1)\phi_j'(L_1)+\left(m_2+\frac{M}{2}\right)g\cos\alpha\cdot L\phi_i'(L)\phi_j'(L),\quad i,j=1,\ldots,n, \tag{26}$$

as symmetric mass coefficient and stiffness coefficient matrices, respectively. Assuming further the material damping of the system as the Rayleigh damping, the damping matrix can be expressed as a linear combination of the mass and stiffness matrices of the form

$$C_{ij} = \hat{\alpha} M_{ij} + \hat{\beta} K_{ij}, \quad i,j = 1,\ldots,n. \tag{27}$$

where $\hat{\alpha}$ and $\hat{\beta}$ are to be determined for different material and/or experiments. With the assumed $M_v(t) = c \cdot \widetilde{V}(t)$ in Eq. (20), one can cast the external force, RHS of Eq. (28), into the form

$$F_i \cdot \widetilde{V}(t) = M_v(t) \cdot [\phi_i'(x_2) - \phi_i'(x_1)] + m_1 g \sin\alpha \cdot \phi_i(L_1) + \left(m_2 + \frac{M}{2}\right) g \sin\alpha \cdot \phi_i(L) \tag{28}$$

with the coefficient F_i as

$$F_i = c \cdot [\phi_i'(x_2) - \phi_i'(x_1)] + \frac{m_1 g \sin\alpha \cdot \phi_i(L_1) + (m_2 + M/2) g \sin\alpha \cdot \phi_i(L)}{Volt(t)}. \tag{29}$$

Finally, the decomposed equations of motion for analysis can be expressed as

$$M_{ij}\ddot{q}_j(t) + C_{ij}\dot{q}_j(t) + K_{ij}q_j(t) = F_i \cdot \widetilde{V}(t), \quad i,j = 1,\ldots,n. \tag{30}$$

where $\{M_{ij}, C_{ij}, K_{ij}\}$ are given by Eqs. (6),(18),(25),(27) and (26) and F_i is given by Eq. (29). With the discrete model in Eq. (30) via the Rayleigh–Ritz decomposition method, the solutions of generalized coordinates $q_j(t)$'s can be easily obtained. One can subsequently utilize the original assumed expression of $y(x, t)$ in Eq. (1) with the assumed-modes in Eq. (3) to derive the flexural motion of piezoelectric bimorph beam, further rendering the translational motions of the platform—the same as that of the beam tip.

2.2. Experimental verification of the predicted beam dynamics

Experiments are conducted to obtain practical frequency response of the piezoelectric feeder. The results are compared with those theoreticals predicted by the dynamic model established in the last subsection. The critical dimensions and material properties of the feeder are listed in Table 1. In addition, the masses of the platform M, and top/lower mounting bolt assemblies, m_1 and m_2 (as shown in Fig. 1) are calibrated, resulting in $M = 0.1057$ kg, $m_1 = 0.0046$ kg and $m_2 = 0.0038$ kg, respectively. The experiment system is set up as shown in Fig. 4a, where the inter-relation between the feeder and equipments is illustrated. The dynamic signal analyzer provides swept-sine input voltages to the piezoelectric patches, ranging from 10 Hz to 1 kHz—the upper operation limit. The input voltage is powered by an amplifier before it is sent to the piezo-patches. With the top platform of the feeder in harmonic translational motions and the part under transporting, a laser displacement sensor is utilized to measure the horizontal displacement of the feeder. Measurements are taken and feedbacked to the dynamic signal analyzer. Calculated by the analyzer, the gain and phase of the frequency response from the applied voltage to the horizontal displacement of the platform can be obtained, which are shown in Fig. 4b, along with the theoretical response. As to the numerical simulated responses, they are obtained based on the derived discrete version of the mathematical model in Eq. (30) with the practical parameters in Table 1 employed. Considering the first three modes; i.e., $n = 1, \ldots, 3$ and assuming $\hat{\alpha} = 0.05$ and $\hat{\beta} = 6 \times 10^{-5}$ for the Rayleigh damping C_{ij}'s defined in Eq. (27), the gain and phase of frequency responses are calculated and also shown in Fig. 4b. Note that due to the non-zero tilting angle of the piezo-beam to the vertical, the transverse flexural direction of the piezo-beam is not in horizontal. Therefore, the theoretically-calculated gain shown in Fig. 4b is multiplied by the cosine of the tilting angle of the piezo-beam to reflect actual beam tip flexural motion before plotted in Fig. 4b.

Table 1
Material properties and dimensions of the piezoelectric feeder

	Piezo-patches	Steel plate	Leaf spring
Total length l (mm)	19	38.9	26
Width b (mm)	13	16	16
Thickness h (mm)	1	2.3	1
Young's modulus E (10^{10}N/m^2)	6.0	20.7	9.56
Density ρ (kg/m^3)	7500	7800	2250
Tilt Angle α (°)	15		
Elastic stiffness c^D (10^{10}N/m^2)	4.22	N/A	N/A
Piezoelectric strain constant d_{31} ($10^{-10}m/V$)	−2.7	N/A	N/A
Piezoelectric stress constant h_{31} (10^8N/Coulomb)	4.39	N/A	N/A
Dielectric impermeability β_{33} (10^6Vm/Coulomb)	6.393	N/A	N/A

It is seen from Fig. 4b that a resonance occurs around 330 Hz, and most importantly, the closeness between the theoretical predicted response and experimental counterpart is clearly present, verifying the effectiveness of the dynamic model established in the previous subsection. Note that the closeness validates that even though the hysteresis effects of the piezo-actuation are not considered by the theoretical model (30), the vibration of the piezo-beam in amplitude can be predicted accurately since the hysteresis induces primarily only the phase shift (time delay) of the piezo-beam response. Therefore, the transported part speed could consequently be accurately estimated. It is also observed from Fig. 4b that the feeder owns fairly flat gain response before the resonance of 330 Hz. This dynamic characteristic allows the piezo-feeder to be usually designed to be operated before or close to the resonance frequency to have fast part-transporting speeds. Finally, Fig. 4c presents the corresponding time-domain experimental and theoretically displacements of the platform in the horizontal direction with input voltage of 150 V and frequency of

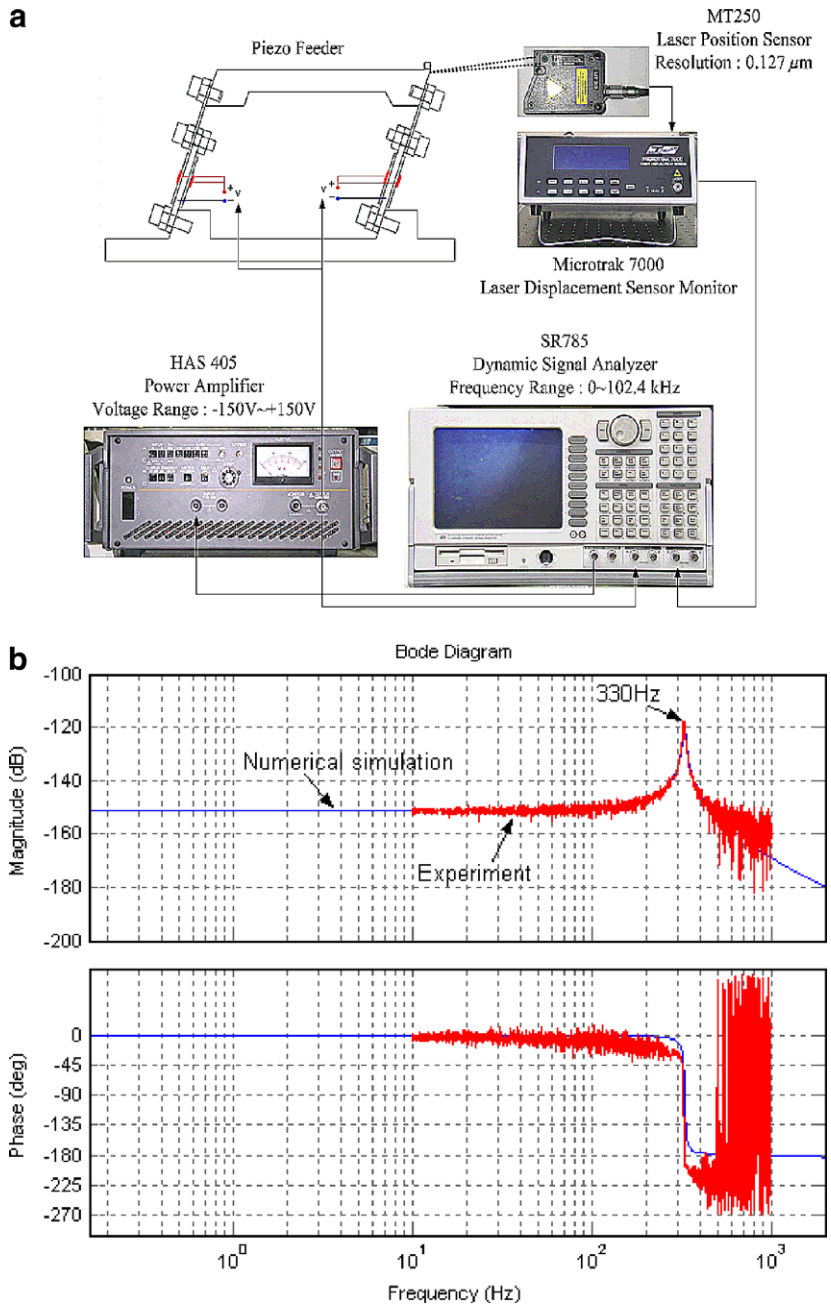

Fig. 4. Experimental verification of platform dynamics; (a) the experiment system for system identification; (b) frequency response of the theoretical and realistic models in horizontal displacement of the vibrating platform; and (c) time-domain horizontal displacement of the platform by experiment and numerical simulation. The input voltage is 150 V in frequency of 250 Hz.

250 Hz. It is seen from this figure that satisfactory correlation between experimentals and theoreticals is clearly present, showing the effectiveness of the established dynamic model in Eq. (30) for predicting dynamics of the platform.

2.3. The impact dynamics of the parts

The interactive dynamics between the transported part and the vibratory platform is explored in this section to find the transporting speed of the part subjected to some harmonic voltage applied. Consider first a horizontal platform supported by a pair of tilted parallel bimorph piezoelectric beams as shown in Fig. 5, where the platform is excited to undergo oscillatory pure translational motions along Y-direction—the motions between solid-lined and dashed-lined positions. These oscillations of the platform in Y-direction first bring the transported part upward along the Y-direction as the platform in uprising, and then allow the part in free falling as the platform is descending. While the platform changing its oscillatory direction from descending to ascending, the transported part has intermittent impacts with the platform until the platform brings the part upward again. In summary, the interactive dynamics between the transported part and the platform can be

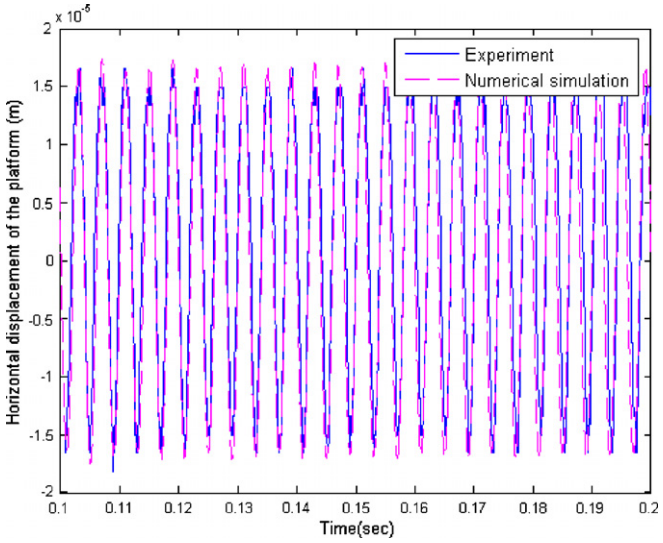

Fig. 4 (*continued*)

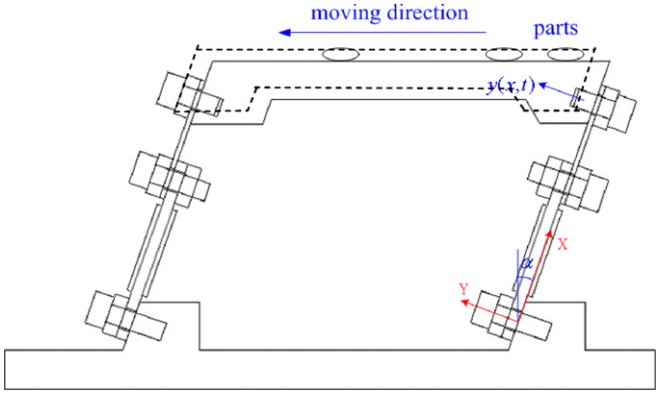

Fig. 5. Parts in transportation on the platform.

divided into three stages: (1) part arising with the platform; (2) part free falling; and (3) part impacting the platform. This series of interactive three-stage dynamics is repeated between platform oscillation cycles, moving the part from one end to another end of the platform. To predict the transporting speed of the part, the following dynamic analysis is conducted. Assuming first the input voltage to the bimorph piezo-beam is in a harmonic form $\widetilde{V}(t) = \bar{V}\sin(2\pi f \cdot t)$, where f is the oscillation frequency in Hz and $\bar{V}$ is the magnitude of the input voltage. The motion of the beam tip in the Y-direction is then also in a harmonic form of

$$y(L_2,t) = A\sin(2\pi f \cdot t), \tag{31}$$

where A is the amplitude of the beam tip response, which can be derived by solving Eqs. (29) and (30). Note that A is also amplitude of platform oscillation. With A solved, the horizontal and vertical motions of the platform, equal to that of the beam tip, can be expressed by

$$d_{\mathrm{pl,h}}(t) = y(L_2,t)\cos\alpha = A\sin(2\pi f t)\cos\alpha, \tag{32}$$
$$d_{\mathrm{pl,v}}(t) = y(L_2,t)\sin\alpha = A\cos(2\pi f t)\sin\alpha, \tag{33}$$

where $d_{\mathrm{pl,h}}(t)$ and $d_{\mathrm{pl,v}}(t)$ denote the horizontal/vertical displacements of the platform, respectively; and α is the tilt angle of the piezo-beams. The horizontal and vertical velocities of the platform are then

$$v_{\mathrm{pl,h}}(t) = \dot{y}(L_2,t)\cos\alpha = 2\pi f A\cos(2\pi f \cdot t)\cdot\cos\alpha, \tag{34}$$
$$v_{\mathrm{pl,v}}(t) = \dot{y}(L_2,t)\sin\alpha = 2\pi f A\cos(2\pi f \cdot t)\cdot\sin\alpha, \tag{35}$$

where $v_{\mathrm{pl,h}}(t)$ and $v_{\mathrm{pl,v}}(t)$ denote horizontal/vertical velocities of the platform, respectively. With the motion of platform in hand, the three stages of impact dynamics for the transported part are exploited next.

2.3.1. Part arising with platform

In this stage, the transported part sticks to the platform; therefore, the displacement/velocity of the part are same as the platform. The displacement/speed of the part can be captured by motion of the platform as follows:

$$d_{\mathrm{pa,h}}(t_i) = d_{\mathrm{pl,h}}(t_i), \tag{36}$$
$$d_{\mathrm{pa,v}}(t_i) = d_{\mathrm{pl,v}}(t_i), \tag{37}$$
$$v_{\mathrm{pa,h}}(t_i) = v_{\mathrm{pl,h}}(t_i), \tag{38}$$
$$v_{\mathrm{pa,v}}(t_i) = v_{\mathrm{pl,v}}(t_i), \tag{39}$$

where t_i denotes the arbitrary time instant when the part arises with the platform; $d_{\mathrm{pa,h}}(t_i)$, $d_{\mathrm{pa,v}}(t_i)$, $v_{\mathrm{pa,h}}$ (t_i) and $v_{\mathrm{pa,v}}(t_i)$ denote the horizontal/vertical displacements and speeds of the transported part, respectively.

2.3.2. Part freely falling (separated from platform)

As the part is lifted by the platform toward the highest horizontal position, the vertical motion of the platform decelerates to zero. The vertical acceleration of the platform in this period can be easily be derived from Eq. (33) or (35) as

$$a_{\mathrm{pl,v}}(t) = -(2\pi f)^2 \cdot A\sin(2\pi f \cdot t)\cdot\sin\alpha. \tag{40}$$

It stands a chance that before the platform reaches the highest horizontal position, the acceleration of the platform falls below the gravity; that is,

$$a_{\mathrm{pl,v}}(t) < -g. \tag{41}$$

The above condition gives the moment when the transported part is separated from the oscillating platform and then experiencing free-falling motion. If the condition are not satisfied, the part sticks to the platform all the time, rendering no part transportation. The vertical position and speed of the part after separation are, respectively, as follows:

$$d_{\mathrm{pa,v}}(t_i) = d_{\mathrm{pa,v}}(t_{i-1}) + v_{\mathrm{pa,v}}(t_{i-1})\cdot(t_i - t_{i-1}) - \frac{1}{2}g\cdot(t_i - t_{i-1})^2, \tag{42}$$
$$v_{\mathrm{pa,v}}(t_i) = v_{\mathrm{pa,v}}(t_{i-1}) - g(t_i - t_{i-1}), \tag{43}$$

where $\{t_i, t_{i-1}\}$ are two arbitrary time instants during part free-falling. As to the horizontal motion of the part, it is a constant motion after the separation. In the other words, the horizontal speed of the part maintains the last speed

as separated from the platform; therefore, the horizontal position and speed of the part after separation are, respectively, as follows:

$$d_{\mathrm{pa,h}}(t_i) = d_{\mathrm{pa,h}}(t_{i-1}) + v_{\mathrm{pa,h}}(t_{i-1}) \cdot (t_i - t_{i-1}), \tag{44}$$

$$v_{\mathrm{pa,h}}(t_i) = v_{\mathrm{pa,h}}(t_{i-1}). \tag{45}$$

2.3.3. Part impacting the platform

As the platform decelerates its vertical motion to complete almost an oscillation cycle, the free-falling part with a constant downward acceleration of gravity is bound to impact the platform. Assuming negligible horizontal friction between the part and platform, it can be deducted that with the platform kept in horizontal, the impact only affects the vertical motions of the part before and after the impact; i.e., the horizontal part-transporting speed are the same around the impact instant. Based on the aforementioned, the basic theory of one-dimensional collision [21] with coefficient of restitution e being employed to characterize the impact dynamics of the transported part, which asserts the principle

$$(v_1' - v_2') = -e \cdot (v_1 - v_2), \tag{46}$$

where v_1' and v_2' are the velocities of the colliding objectives after impacting, and v_1 and v_2 are the velocities of the objects before impacting. Applying principle (48) and conservation of momentum, the after-impact vertical velocities of the part and the platform can be derived, respectively, as

$$v'_{\mathrm{pa,v}}(t_i) = \frac{(m_{\mathrm{pa}} - eM) \cdot v_{\mathrm{pa,v}}(t_i) + M(1+e) \cdot v_{\mathrm{pl,v}}(t_i)}{(m_{\mathrm{pa}} + M)}, \tag{47}$$

$$v'_{\mathrm{pl,v}}(t_i) = \frac{m_{\mathrm{pa}}(1+e) \cdot v_{\mathrm{pa,v}}(t_i) + (M - em_{\mathrm{pa}}) \cdot v_{\mathrm{pl,v}}(t_i)}{(m_{\mathrm{pa}} + M)}, \tag{48}$$

where m_{pa} and M denote the masses of the parts and the platform; $v_{\mathrm{pa,v}}(t_i)$ and $v_{\mathrm{pl},v}(t_i)$ are the velocities of the part and the platform before impact, respectively; $v'_{\mathrm{pa,v}}(t_i)$ and $v'_{\mathrm{pl,v}}(t_i)$ represent the ones after impact. Assuming mass of the platform is much larger than that of the transported part; i.e., $M \gg m_{\mathrm{pa}}$, the after-impact velocities of the platform and transported part in Eqs. (47) and (48) can be well approximated by

$$v'_{\mathrm{pa,v}}(t_i) = -e \cdot v_{\mathrm{pa,v}}(t_i) + (1+e) \cdot v_{\mathrm{pl,v}}(t_i), \tag{49}$$

$$v'_{\mathrm{pl,v}}(t_i) = v_{\mathrm{pl,v}}(t_i). \tag{50}$$

Eq. (50) indicates that the motion of the platform is unaffected by the part impact. This justifies the dynamic modeling of the piezo-beam in Section 2.1 to leave out the dynamic influence from part impacting. On the other hand, as the friction is neglected in horizontal, the horizontal velocity of the part is the same before and after the impact, that is,

$$v_{\mathrm{pa,h}}(t_i) = v_{\mathrm{pa,h}}(t_{i-1}). \tag{51}$$

With the dynamic modeling accomplished for the piezo-beams and transported part in Section 2, simulations are conducted in the following steps to predict the part-transportation speed. Suppose first the part and the platform are both initially still. In the first stage the input voltage of $\widetilde{V} = \bar{V}\sin(2\pi f \cdot t)$ is applied to the piezo-patches of the platform to raise the part up until the downward acceleration of the platform exceeds gravity. After this happens, in the second stage, the part is separated from the platform and in free falling. As the downward speed of the platform further decelerates, the parts will impact intermittently with the platform in the third stage until the part sticks with the platform again. Then the simulation repeats itself from the first stage until the designated end of simulation period. In this way of simulation, the motions of the part and platform are solved, and finally the average transport velocity of the part on the piezo-feeder can be computed by

$$\bar{v}_t = \frac{\int_T^{T+\Delta T} v_{\mathrm{pa,h}}(t)\mathrm{d}t}{\Delta T}, \tag{52}$$

where T and ΔT are initial time and period of simulation, respectively.

3. Numerical simulation and experiment verification

Experiments are conducted to verify the effectiveness of the previously-established mathematical models for predicting the transporting velocity of the part. The practical part feeder and the experiment system for measuring part-transporting speed are shown in Fig. 6. The signal generator is used to generate sinusoidal input signals, which are amplified by a power amplifier to vibrate the piezo-feeder. A laser displacement sensor (MT250) is used to measure the horizontal/vertical motions of the vibratory platform for dynamic verification. Due to the fact that the part in transportation is in high-frequency up-and-down motions and its size is usually small, it is highly difficult to keep pointing the laser beam of the non-contact displacement sensor right at the transported part for measuring part displacement. To overcome the difficulty, a CCD camera is instead utilized to record the part-transportation motion for the purpose of estimating transporting speed. The dimensions and material properties of the piezo-feeder are shown as in Table 1. The input frequency range is usually 60–300 Hz to be below and close to the resonance of 330 Hz, as found in Fig. 4b. The feeder is operated under the resonance frequency of 330 Hz to avoid structural break-down. The test part to be transported is a small screw weighted 1 g; i.e., $m_{\mathrm{pa}} = 0.001$ kg. The coefficient of restitution for collision is identified as $e \approx 0.3$ based on a simple drop test.

Setting the input voltage as 230 V and 150 V in the same frequency of 250 Hz, theoretical responses of the platform and part are computed based on the discrete dynamic Eq. (30) featuring the first three modes. Figs. 7 and 8 show the resulted time responses, respectively, for cases of 230 V and 150 V, respectively. Fig. 7a presents the simulated displacements of the platform and part over two oscillating cycles of the platform. In this figure, the critical

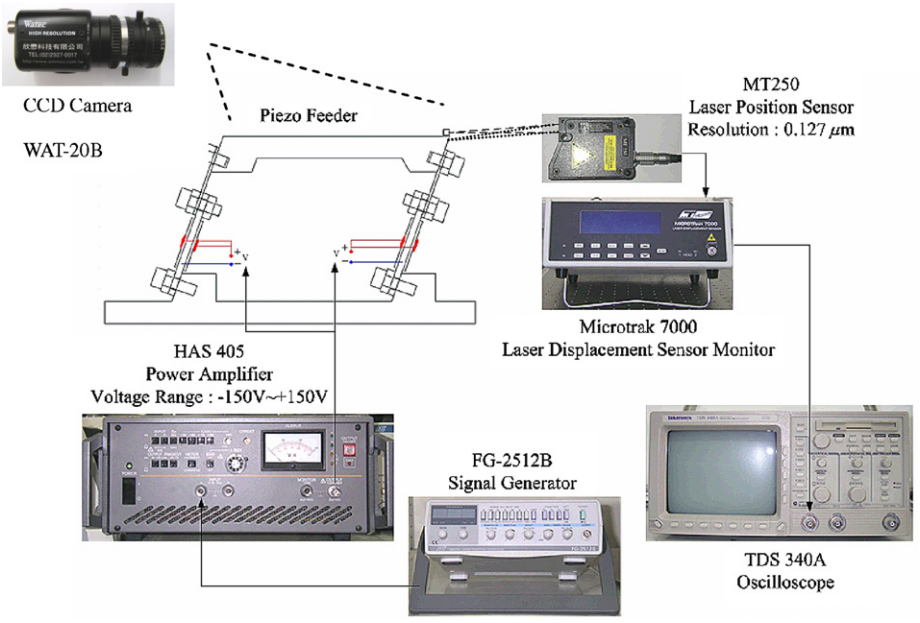

Fig. 6. Experiment system for measuring motions of the platform and the transported part.

times denotes when the part is separated from the platform and when collisions occur. It is seen from this figure that the part is separated from the oscillating platform around 0.4 ms before the platform reaches its highest position. The separation timing is in fact right at the moment the gravity is equal to the vertical acceleration of the platform, as evident from Fig. 7b. It is also seen from Fig. 7a that after the part is separated from the platform, the part falls freely until it collides with the platform around 3.1 ms. With several collisions, the part sticks with the platform again after approximately 3.7 ms, then starting another round of stiction with the platform, separation and collisions. As to the horizontal displacement of the transported part—the transportation distance of the part, it can be deducted that the part moves horizontally with the platform in the period of stiction, while it undergoes horizontal motion in a contact velocity in periods of free-falling and collisions. Therefore, the horizontal displacement of the transported part can be easily obtained and depicted in Fig. 7d, where between the separation and the last collision the part displacement conforms to a constant velocity horizontal motion, while between the last collision and separation the horizontal displacement of the part is the same as that of the platform, as shown in Fig. 7e. Finally, the transported velocity of the part is obtained by differentiating the previously-computed horizontal displacement of the part in Fig. 7d. The results are shown in Fig. 7e. Making use of the results in Fig. 7e, where it is seen that it can be computed that the averaged transporting speed is 34 mm/s. For another case with less input voltage of 150 V, the previous analysis/computation are conducted again to observe the effects of level of input voltage on the transportation speed. The same computations as those for input voltage of 230 V are carried out to present the results in Fig. 8a–e. A scrupulous comparison between Figs. 7 and 8 reveals that the smaller input voltage of 150 V leads to a longer period of part stiction to the platform (as shown in Fig. 8a), and results in slower averaged transportation speed of 6.85 mm/s (as shown in Fig. 8e). Therefore, a general rule of maximizing the part traveling speed is to increase the input voltage for a shorter period of part stiction to the platform.

In order to verify the effectiveness of the theoretical models established previously for platform vibration and part transportation, theoretical transportation motions of the part over the full length of the platform are next computed, along with one single run of experimental displacements of the transported part measured by a CCD camera. The results are shown in Fig. 9a, where the solid curve represents theoretical predictions, while the asterisks denote the measured traveling distances of the transported part by a CCD camera. Also shown in this figure are the traveling times of the part over the total length of the platform—5.01 and 4.96 s from experiments and theoretical predictions, respectively. Note that the solid curve is in fact combination of thousand of cycles of horizontal part displacements shown in Fig. 8d that lasts 0.008 s. It can be generally seen from Fig. 9a that the closeness between the theoreticals and experimentals are clearly present, showing the effectiveness of the theoretical models established in this study.

It should be noted at this point that the measured traveling motion of the part in fact varies from run to run, possibly due to the facts that the transported screw is not a point mass as assumed and the existence of friction in horizontal direction that was not considered. For further confirmation on prediction accuracy in part-transporting speed, one hundred runs of part traveling for the total platform length of 34 mm are conducted with the CCD camera to record the total traveling time. Fig. 9b depicts the

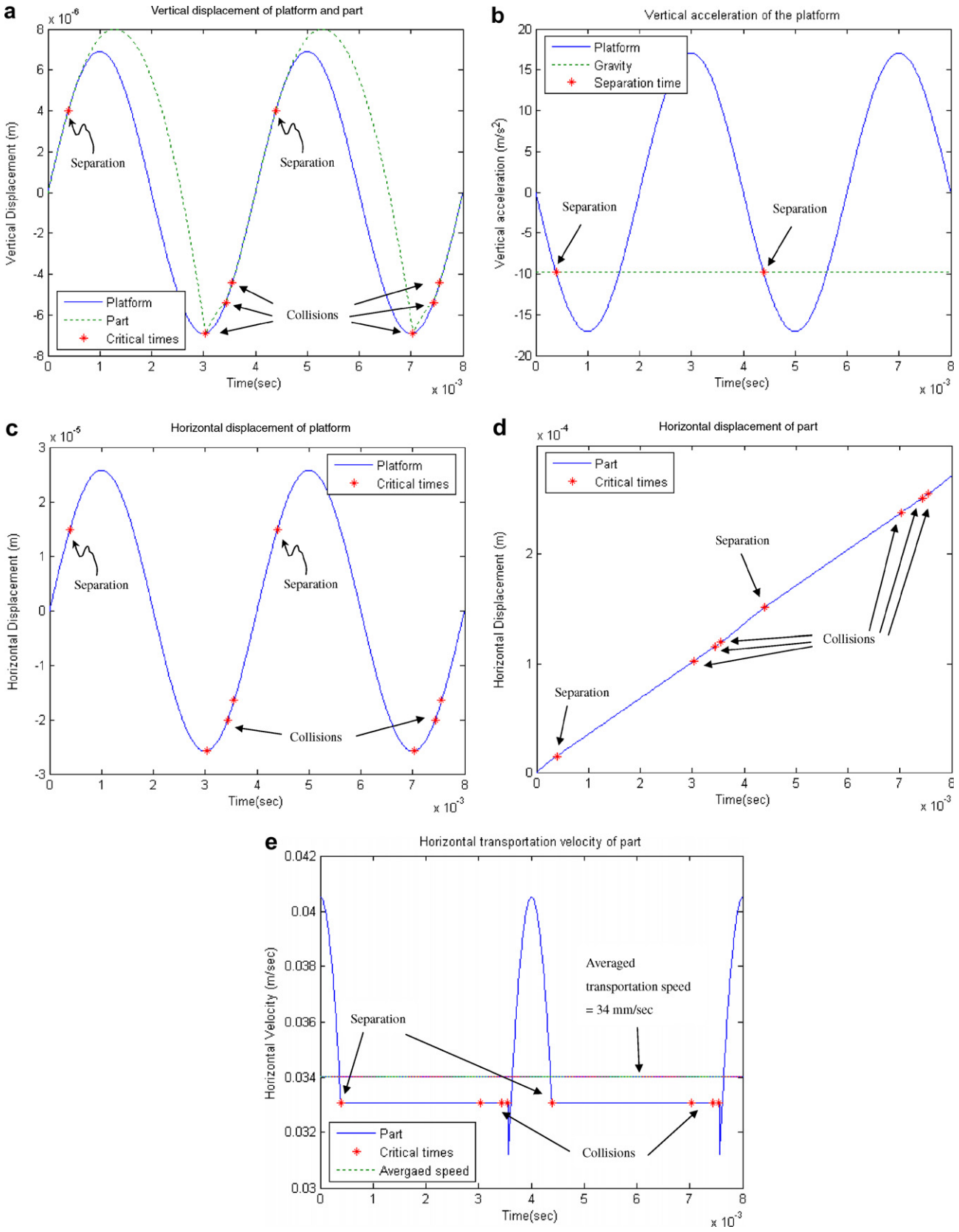

Fig. 7. Simulated responses of the platform and part subjected to input voltage of 230 V in frequency of 250 Hz: (a) vertical displacement of the platform and part; (b) vertical acceleration of the platform; (c) horizontal displacement of the platform; (d) horizontal displacement of the transported part; and (e) transportation speed of the part.

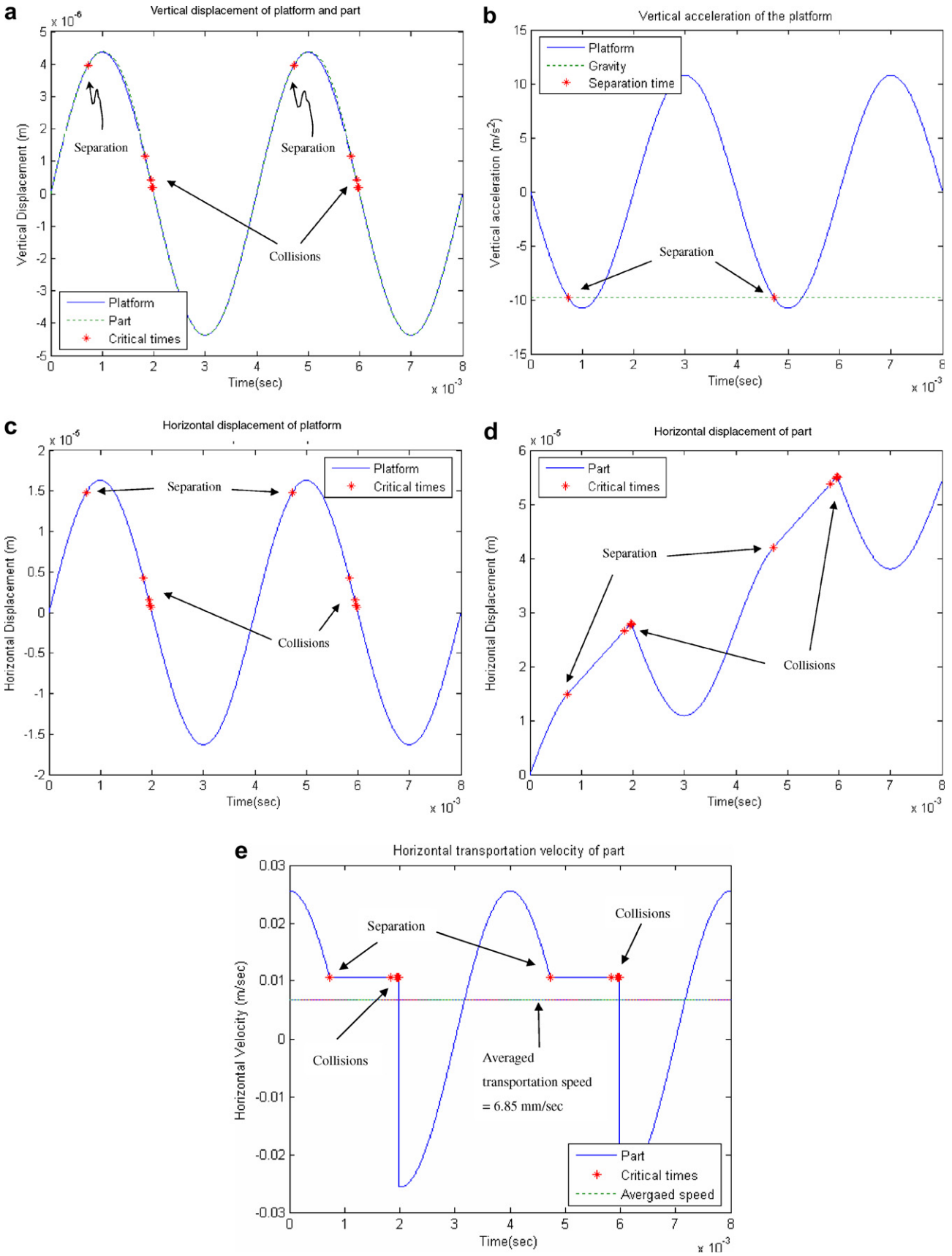

Fig. 8. Simulated responses of the platform and part subjected to input voltage of 150 V in frequency of 250 Hz: (a) vertical displacement of the platform and part; (b) vertical acceleration of the platform; (c) horizontal displacement of the platform; (d) horizontal displacement of the transported part; and (e) transportation speed of the part.

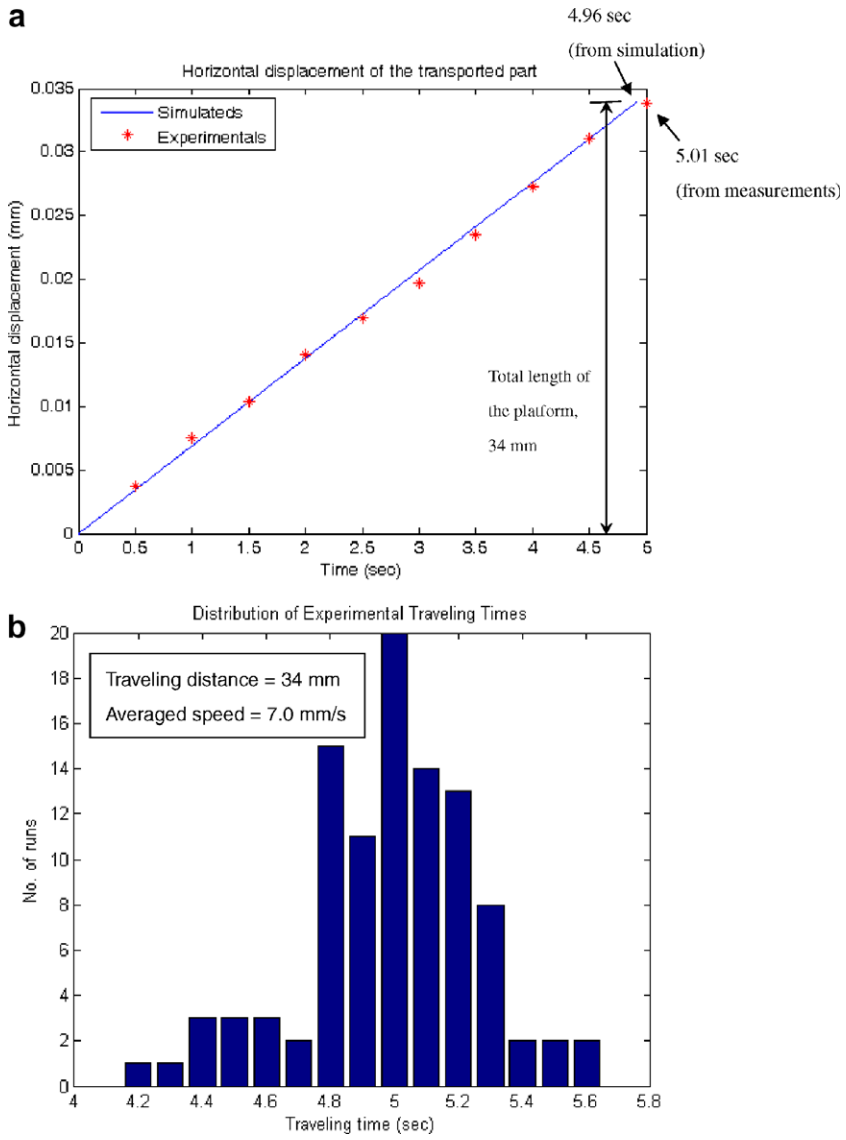

Fig. 9. Traveling history of the transported part subjected to input voltage of 150 V in frequency of 250 Hz: (a) time history of part traveling distance for a particular run—horizontal displacement over the length of the platform, 34 mm; (b) distribution of experimental traveling times over the total length of the platform, 34 mm.

distribution of the recorded traveling times for 100 runs in a bar chart. It can be seen from this chart that the distribution of the measured traveling time centers around the theoretically-predicted traveling time, 4.96 s, as shown in Fig. 9a, within an acceptable range, demonstrating the effectiveness of the theoretical model. Furthermore, the theoretically-predicted traveling speed of 6.85 mm/s as shown in Fig. 9a is also close to 7.0 mm/s, the experimental averaged traveling speed herein in Fig. 9b over 100 runs of transportation.

4. Conclusions

A thorough modeling of the piezoelectric part feeder with the aim on predicting part-transporting speed is accomplished in this study. It starts with an establishment of the dynamic equations of motion of the piezo-beams in the piezo-feeder via the Rayleigh–Ritz method and is then followed by the modeling on the impact dynamics between the platform and transported part, which is accomplished via basic collision theory. The validity of the established models is further ensured by experiments. The closeness shown between the theoretically-predicted dynamics of the feeder/part and those experimental counterparts finally confirm the success of the modelings. Based on the analytical and experimental results obtained, the following conclusions can be drawn.

(1) The first three assumed-modes proposed in Eq. (3) are capable of predicting the realistic dynamics of a flexurally-vibrated piezoelectric beam, as evident from the experimental results in Fig. 4b and c.

(2) The basic collision theory is pertinent to be employed to predict the impact dynamics between the platform and transported part, leading to well-predicted part-transporting speeds as evident from Fig. 9a and b.
(3) It is theoretically predicted and experimentally confirmed that the transported part experiences three stages of different types of motions: (1) part arising with the platform; (2) part free falling; and (3) part impacting the platform. This series of interactive three-stage dynamics is repeated between platform oscillation cycles, moving the part from one end to another of the platform. The transported part moves horizontally with the platform in the period of arising with the platform, while it undergoes horizontal motion in a contact velocity in periods of free-falling and collisions.
(4) A few general rules for control strategy have been distilled:
   i. Based on experimental operation, the feeder should be operated under the resonance frequency of 330 Hz to avoid structural break-down.
   ii. A basic rule of maximizing the part traveling speed is to increase the input voltage for a shorter period of part stiction to the platform.

Although the part-traveling speeds theoretically predicted in this study anticipate well about the realistics, a broader distribution range of experimental part-traveling speeds as compared to the theoreticals is present, as shown in Fig. 9b. This might be due to the facts that (1) the transported part is not a point mass and (2) the ignorance on the impact friction between the part and platform. To further improve modeling, the part needs to be assumed as a rigid body and one needs to investigate the dynamic effects of the impact friction on the part-transporting speed in the future.

Acknowledgements

The authors are greatly indebted to the National Science Council of ROC for the support of the research through Contract Nos. 95-2221-E-009-367 and 95-2745-E-033-004-URD.

References

[1] P. Ge, M. Jouaneh, Modeling hysteresis in piezoceramic actuators, Precision Engineering 17 (3) (1995) 211–221.
[2] M. Goldfarb, N. Celanovic, Modeling piezoelectric stack actuators for control of micromanipulation, IEEE Transactions on Control Systems (1997) 69–79.
[3] D. Croft, G. Shed, S. Devasia, Creep, hysteresis, and vibration compensation for piezoactuators: atomic force microscopy application, ASME Journal of Dynamic Systems, Measurement 123 (2001) 35–43.
[4] P. Ge, M. Jouaneh, Tracking control of piezoceramic actuator, IEEE Transactions on Control Systems Technology 4 (3) (1996) 209–216.
[5] S.B. Jung, S.W. Kim, Improvement of scanning accuracy of PZT piezoelectric actuators by feed-forward model-reference control, Precision Engineering 16 (1) (1994) 49–55.
[6] S.B. Choi, S.S. Cho, Y.P. Park, Vibration and position tracking control of piezoceramic-based smart structures via QFT, ASME Journal of Dynamic Systems, Measurement, and Control 121 (1999) 27–32.
[7] S.B. Choi, H.K. Kim, S.C. Lim, Y.P. Park, Position tracking control of an optical pick-up device using piezoceramic actuator, Mechatronics 11 (2001) 691–705.
[8] S.B. Choi, H.C. Shin, A hybrid actuator scheme for robust position control of a flexible single-link manipulator, Journal of Robotic Systems 13 (6) (1996) 359–370.
[9] S.B. Choi, C.C. Cheong, B.S. Thompson, M.V. Gandhi, Vibration control of flexible linkage mechanisms using piezoelectric films, Mechanism and Machine Theory 29 (4) (1994) 535–546.
[10] S.V. Gosavi, G. Kelkar, Modeling identification, and passivity-based robust control of piezo-actuated flexible beam, ASME Journal of Vibration and Acoustics 126 (2) (2004) 260–271.
[11] J.H. Han, K.H. Rew, I. Lee, An experimental study of active vibration control of composite structures with a piezo-ceramic actuator and a piezo-film sensor, Smart Materials and Structure 6 (1997) 549–558.
[12] T. Bailey, J.E. Hubbard Jr., Distributed piezoelectric-polymer active vibration control of a Cantilever beam, AIAA Journal of Guidance and Control 8 (5) (1985) 605–611.
[13] V. Piefort, A. Preumont, Finite element modeling of piezoelectric structures, Samtech User's Conference, January 2001.
[14] D.J. Cappelleri, M.I. Frecker, T.W. Simpson, Optimal design of a PZT bimorph actuator for minimally invasive surgery, in: Proceedings of SPIE, vol. 3984, 2000, pp. 321–335.
[15] R.F. Fung, S.C. Chao, Y.S. Kung, Piezothermoelastic analysis of an optical beam deflector, Sensors and Actuators A: Physical 87 (2001) 179–187.
[16] R.F. Fung, S.C. Chao, Dynamic analysis of an optical beam deflector, Sensors and Actuators A: Physical 84 (2000) 1–6.
[17] S.B. Choi, D.H. Lee, Modal analysis and control of a bowl parts feeder activated by piezoceramic actuators, Journal of Sound and Vibration 275 (2004) 452–458.
[18] W.H. Jiang, P.S.K. Chua, F.L. Tan, Simulation software for parts feeding in a vibratory bowl feeder, International Journal of Production Research 41 (9) (2003) 2037–2055.
[19] T. Doi, K. Yoshida, Y. Tamai, K. Kono, K. Naito, T. Ono, Feedback control for electromagnetic vibration feeder, JSME International Journal, Series C 44 (1) (2001) 44–52.
[20] L. Meirovitch, Fundamentals of Vibrations, McGraw Hill Int., New York, USA, 2001.
[21] A.P. Boresi, R.J. Schmidt, Engineering Mechanics: Dynamics, Brooks/Cole, CA, USA, 2000.